A Comparison of Functional and Structural Consequences of the Tyrosine B10 and Glutamine E7 Motifs in Two Invertebrate Hemoglobins (*Ascaris suum* and *Lucina pectinata*)†

Eric S. Peterson,‡ Shuocai Huang,‡ Jiaqian Wang,‡ Lisa M. Miller,‡ Gediminas Vidugiris,‡,§ Andrew P. Kloek,‖ Daniel E. Goldberg,‖ Mark R. Chance,‡ Jonathan B. Wittenberg,‡ and Joel M. Friedman*,‡

Department of Physiology and Biophysics, Albert Einstein College of Medicine, Bronx, New York 10461, and Howard Hughes Medical Institute and Departments of Medicine and Molecular Microbiology, Washington University School of Medicine, St. Louis, Missouri 63110

Received May 16, 1997; Revised Manuscript Received July 28, 1997⊗

ABSTRACT: The architecture of the distal heme pocket in hemoglobins and myoglobins can play an important role in controlling ligand binding dynamics. The size and polarity of the residues occupying the distal pocket may contribute steric and dielectric effects. In vertebrate systems, the distal pocket typically contains a "distal" histidine at position E7 and a leucine at position B10. There are several invertebrate organisms that have hemoglobins or myoglobins that display a pattern in which residues E7 and B10 are a glutamine and tyrosine, respectively. These proteins often have very high oxygen affinities stemming from very slow ligand off rates. In this study, two such hemoglobins, one from the nematode *Ascaris suum* and the other from the sulfide-fixing clam *Lucina pectinata*, are compared with respect to conformational and functional properties. Ultraviolet resonance Raman spectroscopy and visible resonance Raman spectroscopy are used to probe, respectively, the ligand-dependent hydrogen bonding pattern of the tyrosine residues and the proximal heme pocket interactions. Fourier transform infrared absorption spectroscopy is used to probe the dielectric properties of the distal heme pocket through the stretching frequency of carbon monoxide bound to the heme. Functionality is probed through the geminate rebinding of both CO and O_2. The findings reveal two very different patterns indicative of two different mechanisms for achieving low oxygen off rates. In Hb Ascaris, a hydrogen bonding network that includes the E7 Gln, B10 Tyr, and oxygen bound to the heme results in a tight cage for the oxygen. Dissociation of the O_2 requires a large amplitude conformational fluctuation that results both in a spontaneous dissociation of the oxygen through the loss of hydrogen bond stabilization and in an enhanced probability for ligand escape though the transient disruption and opening of the tight distal cage. In the case of the Hb from *Lucina*, there is no evidence for a tight cage. Instead the data support a model in which the hydrogen bonding network is far more tenuous and the equilibrium state of distal pocket is far more open and accessible than is the case in *Ascaris*. The results explain why Hb Ascaris has one of the highest oxygen affinities known ($P_{50} \sim 10^{-3}$ Torr) while Hb Lucina II has an oxygen affinity comparable to that of Mb ($P_{50} = 0.13$ Torr) even though both of these Hbs contain the B10 Tyr and E7 Gln motif and display very low oxygen off rates. The roles of water and proximal strain are discussed.

Ligand binding to hemoglobins and myoglobins is a model protein reaction that has been the focus of much research. Despite the seeming simplicity of the reaction, research has revealed many layers of complexity associated with this process. One very basic issue is how the protein surrounding the ligand binding site controls reactivity. Protein control of ligand binding reactivity is divided into two broad categories based on the architecture of the ligand binding site in heme proteins: proximal control and distal control.

The ligand binding site is composed of the heme, to which the ligand binds reversibly, and of the surrounding globin. In addition, water molecules may also be localized within the interior of the protein near or at the ligand binding site. In most instances, the heme is covalently coupled to the globin through an iron−histidine bond. This "proximal histidine", an invariant residue in hemoglobins and myoglobins, is usually the seventh or eighth residue on the F helix. Control of ligand reactivity through protein modulation of the iron displacement from the heme plane via manipulation of the heme−proximal histidine stereochemistry or electronic properties is termed proximal control. If one views the heme cavity as being divided by the plane of the heme porphyrin, the portion of the heme cavity containing the F helix and the proximal histidine is termed the proximal heme pocket. The opposite side of the heme cavity is termed the distal heme pocket.

The distal heme pocket defines the environment of the iron-bound ligand as well as the environment of the ligand both immediately after dissociation and just prior to binding. Control of ligand binding reactivity through the residues of the distal heme pocket is referred to as distal control. Two important distal pocket residues that have been shown to play

† This work was supported in part by National Institutes of Health Grants R01GM44343 (J.M.F.), P01HL51084 (J.M.F.), R01HL58247 (J.M.F.), HL45892 (M.R.C.), and RR01633 (M.R.C.), and by the W. M. Keck Foundation.

* Corresponding author. Fax: 718-430-8819. Email: jfriedma@aecom.yu.edu. Telephone: 718-430-3591.

‡ Albert Einstein College of Medicine.

§ Present address: Department of Pharmacology, University of Wisconsin, Madison, WI 53706.

‖ Washington University School of Medicine.

⊗ Abstract published in *Advance ACS Abstracts,* October 1, 1997.

S0006-2960(97)01156-2 CCC: $14.00

a potentially significant role in modulating ligand reactivity are E7 and B10 (Carver et al., 1992; Carlson et al., 1994; Gibson et al., 1992; Rohlfs et al., 1990; Springer et al., 1994). In most vertebrate Hbs and Mbs, these residues are a histidine and a leucine, respectively. There are, however, a small but significant number of naturally occurring proteins, primarily in invertebrates, that have the histidine and leucine replaced by a glutamine and a tyrosine, respectively. The ligand binding properties of many of these atypical proteins are extreme. In this study, two such hemoglobins, one from the nematode *Ascaris suum* and the other from the sulfide-fixing clam *Lucina pectinata*, are examined and compared in an attempt to better understand the possible role these residues play in conferring the extreme ligand binding properties to Hbs and Mbs.

A. suum, a parasitic nematode, has a perienteric hemoglobin with an oxygen affinity up to 10^4 times higher than that of vertebrate globins ($P_{50} = 0.004$ Torr in contrast to ~0.5−30 Torr for other Hbs or Mbs). In striking contrast, the affinity of the protein for carbon monoxide is the same as that found in vertebrate hemoglobins and myoglobins ($P_{50} \sim 0.1$ Torr) (Davenport, 1949; Okazaki & Wittenberg, 1965). The high oxygen affinity arises from an exceptionally slow oxygen dissociation rate (3000 times lower than for vertebrate Mb) (Davenport, 1949).

Ascaris hemoglobin consists of eight identical subunits, with each subunit containing two myoglobin-like domains (D1 and D2) in tandem, one of which contains a highly charged C-terminal tail, which is probably involved in octamerization (De Baere et al., 1992; Perutz et al., 1993; Kloek et al., 1993; Sherman et al., 1992). Domain 1 of Ascaris Hb has recently been cloned and expressed in *Escherichia coli* by Goldberg and co-workers (Kloek et al., 1993; Sherman et al., 1992). It was found that the isolated monomeric domain retains the high O_2 affinity of the intact octamer, demonstrating that the affinity is intrinsic and at least relatively independent of subunit interaction. Alignment of the individual domains with vertebrate globins typically shows only about 15% homology, yet numerous invariant residues have been found (De Baer et al., 1992; Sherman et al., 1992).

As stated above, one important difference between Ascaris Hb and most vertebrate oxygen carriers is that the distal histidine E7 found in vertebrate globins is replaced with a glutamine in both Ascaris hemoglobin domains. The distal histidine is a well-studied residue known to stabilize the heme-bound oxygen through a hydrogen bond (Phillips & Schoenborn, 1981; Nagai et al., 1987; Braunstein et al., 1988; Springer et al., 1994). Glutamine, the most common naturally occurring replacement for histidine, can also serve as a hydrogen bond donor to the bound oxygen in Ascaris Hb. Indeed, conversion of this residue to leucine or alanine produces a D1 hemoglobin variant with oxygen off rates 5- and 60-fold higher, respectively, than that of the wild-type D1 (Kloek et al., 1994). These rates are still 2 or 3 orders of magnitude lower than in vertebrate proteins. Thus, glutamine substitution alone cannot account for the drastic reduction in the oxygen off rate.

There is evidence for an additional hydrogen bond to the bound oxygen in the Ascaris distal pocket originating from the tyrosine residue at position B10. Mutation of this residue to either phenylalanine or leucine greatly increases the off rate of oxygen, resulting in more than a 100-fold decrease in oxygen affinity (Kloek et al., 1994; De Baere et al., 1994). The above studies suggest that the glutamine and tyrosine side chains in the heme pocket stabilize the heme-bound oxygen, with hydrogen bonding being the likely mechanism. Surprisingly, the sperm whale myoglobin mutant where the native B10 leucine is replaced by a tyrosine has a decreased oxygen affinity, with an off rate 50 times higher than that of the wild type (Gibson et al., 1993), illustrating the fundamental limitations of identifying the structural or functional role of residues based solely on the site-directed mutagenesis approach.

Ultraviolet (UV) resonance Raman spectroscopy has been used to directly observe the formation of this hydrogen bond upon oxygen binding (Huang et al., 1996). This study revealed that both oxygen and carbon monoxide induce similar protein conformational changes in the globin upon binding to the heme; however, in the case of oxygen, a strong hydrogen bond involving tyrosine as the proton donor was also observed. The results obtained on the E7 Gln→Leu mutant of this Hb suggest that the glutamine plays a role in stabilizing a rigid tertiary structure associated with the distal heme pocket. An X-ray structure of the oxy derivative indicates that the glutamine, tyrosine, and oxygen are sufficiently close to form a tight hydrogen bonding network (Yang et al., 1995). This conformation most likely maintains the tyrosine in an orientation conducive to hydrogen bond formation with a heme-bound oxygen, whereas in the Mb B10 Leu→Tyr mutant, the tyrosine is not in an optimal orientation for the formation of the stabilizing hydrogen bond.

The symbiont-harboring gills of the clam *L. pectinata* contain a cytoplasmic hemoglobin (Hb-II) that exhibits moderately high oxygen affinity ($P_{50} = 0.13$ Torr) and unusually slow rates for oxygen dissociation (Kraus & Wittenberg, 1990; Hockenhull-Johnson et al., 1991). The CO affinity is slightly lower than that of mammalian Mbs [the CO P_{50} value is not published, but the CO dissociation equilibrium constant is 370 nM, compared to 42 nM for sperm whale Mb (Kraus & Wittenberg, 1990)]. As in *Ascaris* hemoglobin, the distal residues at positions E7 and B10 are glutamine and tyrosine respectively. The B10 tyrosine in this protein has been previously invoked in possible functional roles (Kraus et al., 1990; Hockenhull-Johnson et al., 1991).

Since both Hb-II from *Lucina* and Hb from *Ascaris* have the same E7 and B10 residues as well as a significant reduction in the oxygen off rates, it is reasonable to hypothesize that both proteins exert control over the oxygen dissociation process through the same mechanism. However, the large difference in the O_2 affinities suggests that a distinct difference also exists between the two. The focus of this study is both to determine whether the two hemoglobins do exhibit a similar mechanism for the control of ligand reactivity and to better understand the mechanism(s) through which these distal residues engender the differences in ligand reactivity.

Ultraviolet resonance Raman spectroscopy is used to probe the ligand binding induced changes in the tyrosines and tryptophans in these two proteins. In particular, the focus is on the response of the tyrosine hydrogen bonding pattern to ligand binding (CO and O_2). Visible resonance Raman spectroscopy (Spiro et al., 1988; Rousseau & Friedman, 1988; Friedman, 1994) is used to probe the heme−proximal

histidine linkage. Fourier transform infrared absorption spectroscopy (FTIR) is used to determine whether the tyrosine is sufficiently close to the heme-bound ligand to perturb the CO stretching frequency, a spectral probe of the electrostatic environment of the bound CO (Li et al., 1994; Stavrov 1996, 1997). Geminate recombination (Duddell et al., 1979; Alpert et al., 1979; Friedman & Lyons, 1980) and bimolecular recombination (Antonini & Brunori, 1971) subsequent to laser photodissociation of the bound ligand are used to probe both the barrier for rebinding and the nature of the distal pocket escape/entrance channels.

MATERIALS AND METHODS

UV Resonance Raman Apparatus. The UV resonance Raman excitation source was an intracavity frequency-doubled ring dye laser (Coherent 899) utilizing stilbene 420 pumped by a multi-UV line output of an Argon ion laser (Coherent Innova 400). To maximize the UV output with acceptable bandwidth, a single thin etalon is used instead of the usual two etalons (thick and thin). This laser system generates CW UV output from 218 to 240 nm, and for the experiments herein ~1 mW of 230 nm excitation was used. The scattered photons were collected with a triplet lens (fused Suprasil, CVI Laser Corp.) and focused onto the 270 μm entrance slit of a 1.5 m single monochromator equipped with a 3600 groove/mm holographic grating (Sopra, Inc., France). The detector was a liquid N_2 cooled CCD array with a UV metachrome coating on its chip (Princeton Instruments, Trenton, NJ). The samples (~1 mL) were held in a quartz tube maintained at 10 °C and spun at 5 Hz to minimize local heating and potential photodegradation. The wavenumber shift was calibrated with the use of the Raman spectra of cyclohexane and 1,4-dioxane. For the UV Raman data presented here, spectral acquisitions were carried out as a series of 5 min accumulations. Each final spectrum was the sum of three to five of these 5 min spectra. Before summing the spectra, spectral spikes due to cosmic rays were removed from each spectrum using modified SpectraCalc software (Galactic Industries Corp.). Also, each spectrum was subtracted from the first one taken from a given sample. If difference features were observed, the spectrum was discarded. In order to accurately compare different spectra from different samples, 0.2 M perchlorate was added to the stock buffer solutions from which the samples were prepared. The perchlorate Raman band at 934 cm^{-1} serves as a protein-invariant intensity reference. When comparing two spectra, the spectral intensities from the protein are normalized by matching the heights of the perchlorate internal reference bands at 934 cm^{-1}. This technique is used for accurate comparisons only for those situations where it is possible to maintain the identical concentrations of both perchlorate and protein, as in comparisons between the deoxy and ligand-bound forms of a given protein where all the derivatives are made from the same stock solution. The sample preparation was as described below for the visible Raman experiments, except that the protein concentration was typically ~0.1 mM in heme and in 30 mM, pH 7.3, phosphate buffer and the perchlorate standard was added.

Visible Resonance Raman Spectroscopy. (A) Sample Preparation. CO derivatives were prepared from oxy stock solutions by passing CO gas over the surface of a 100 μL aliquot in a sealed vial. Deoxy derivatives were prepared by passing N_2 over the sample and then adding 5 equiv with respect to heme concentration of sodium dithionite. All samples were approximately 1 mM in heme and in pH 7, 0.1 M potassium phosphate buffer. The samples were then loaded in a nitrogen atmosphere into quartz sample cells with a 200 μm path length. (Helma P/N 124-QS, Jamaica, NY). The front window of the cell was replaced with a sapphire window, which yielded a flatter base line in the low-frequency region of the Raman spectrum. The sample cell was mounted in a custom brass holder, which was cooled to approximately 10 °C and rotated fast enough such that a new sample volume was interrogated with each laser shot. Photoproduct buildup and artifacts from sample spinning were found to be negligible by varying the spinning rate and by taking visible absorption spectra before and after each experiment. This sample preparation and arrangement was used for both the Raman and flash photolysis experiments.

(B) Visible Raman Apparatus. Visible time-resolved resonance Raman spectra were obtained using an 8 ns 435.8 nm pulse to both photodissociate the ligand and Raman scatter off the sample. The laser used was a Nd:YAG laser (Continuum NY81C-20, Santa Clara, CA), which produced 450 mJ pulses at 20 Hz in the second harmonic output at 532 nm. Four watts of the 532 nm beam was focused into a homemade 90 cm long cell filled with 120 psi of hydrogen to Raman shift the laser to 435.8 nm. Neutral density filters were used to reduce the energy of the 435.8 nm pulses to 150 μJ, and these were focused with a 150 mm plano-convex lens on the sample at an incidence angle of 45°. The Raman scattered light was collected at the normal incidence to the sample (135° to the laser) with a 50 mm Nikon F/1.4 camera lens and focused with an f-matching lens onto the 50 μm × 5 mm slit of a 0.64 m single monochromator utilizing an 1800 grooves/mm grating (ISA HR640, Metuchen, NJ). The Rayleigh line was reduced in intensity with a holographic notch filter (Kaiser P/N HNF-1171 centered at 442 nm, Ann Arbor, MI), and a depolarizer (CVI P/N DPL-10, Putnam, CT) was used to scramble the polarization of the collected light and thus eliminate intensity artifacts created by polarization-dependent grating reflectivity. The detector was an intensified diode array run in the cw mode (Princeton Instruments P/N IRY-1024S/B, Trenton, NJ). The total accumulation time per spectrum was typically 30 min. The spectral bandwidth of the monochromator was approximately 2.5 cm^{-1}, and the resolution of the detector array was approximately 0.9 cm^{-1} per pixel. Raman spectra were calibrated using solvent spectra with previously determined peak assignments. A least-squares fit was used to map pixel number into relative wavenumbers (Raman shift). The Raman spectra were base lined using a polynomial fitting routine in LabCalc (Galactic Industries, Salem, NH), normalized using the ν_7 mode band at 673 cm^{-1}, and are presented without smoothing.

Ligand Recombination. The flash photolysis apparatus used for the rebinding rate studies utilized the doubled output of a Nd:YAG laser at 532 nm (Continuum Surelite, Santa Clara, CA) to photolyze the samples and the cw output of a HeCd laser at 441.6 nm (Liconix P/N 4230NB, Santa Clara, CA) to monitor the recombination via changes in sample absorbance. The photolysis pulse was 8 ns in duration and was focused to a diameter of approximately 2 mm on the sample with an 800 mm lens. To achieve 100% photolysis within the illuminated sample volume, the photolysis pulse energy was increased until the amplitude of the signal

saturated, typically requiring approximately 2 mJ per pulse. The unfocused HeCd laser probe beam passed through the sample, collinear with the Nd:YAG beam, was spectrally separated from the 532 nm light using colored glass filters and a single monochromator (Varian P/N AA-5, Palo Alto, CA), and was measured with a photomultiplier tube (Hamamatsu P/N R928, Bridgewater, NJ). For each laser shot, the detector output was digitized with a 500 MHz oscilloscope (LeCroy P/N 7200 with a 7242B time base/sampling head; Chestnut Ridge, NJ), resulting in a trace containing 50 000 points separated by 10 ns. Traces for 100 laser shots were averaged. Identical results were obtained from running the laser at 10 Hz and slowly spinning the sample and by running the laser at 1 Hz and not spinning the sample. The data were converted from transmission to change in absorption by taking a logarithm, subtracting a base line, and normalizing.

FTIR. Fourier transform infrared spectra of room temperature samples of the carbonmonoxy derivatives of Lucina Hb-II, native Hb Ascaris, and the B10 Tyr→Phe mutant of the D1 fragment of Hb Ascaris were obtained using a dry nitrogen purged Mattson Galaxy 5000 FTIR spectrometer. The samples were on the order of 5 mM in heme in 75:25 glycerol/buffer solutions, and the sample cell had a 0.005 cm path length. The presented spectra were ratioed to air, and are the sum of 256 scans at 2 cm^{-1} resolution.

Low-Temperature Quantum Yields for Photodissociation. The yield of deoxy-like photoproduct generated through prolonged illumination of an initial ligand-bound sample at 10 K was achieved using the previously described procedure of Miller et al. (1996). The yields for the O_2 derivatives of the Ascaris and Lucina Hbs were compared to each other and to those from vertebrate Mbs.

Protein Samples. The native and mutant D1 domain proteins were prepared and characterized according to previously described procedures (Kloek et al., 1993). Lucina Hb-II was prepared as previously described (Kraus & Wittenberg, 1990) except that a column of Q-Sephadex first equilibrated with a 10 mM triethanolamine hydrochloride buffer, pH 8.3 at 25 °C, and developed with a gradient of sodium chloride concentration from 0 to 0.3 M replaced the DEAE-Sephadex column used previously. The native perienteric Hb from *Ascaris* was prepared as previously described (Wittenberg et al., 1965) from worms obtained at a slaughterhouse. The solutions used for the spectroscopic and rebinding studies were typically 0.3−0.1 mM in heme in 0.05 M phosphate buffer. Unless otherwise noted, the measurements were conducted at ∼292 K.

RESULTS

UV Resonance Raman (UVRR) Spectra. Figure 1 shows a high-frequency portion of the UVRR spectrum of the deoxy and oxy derivatives of the native perienteric octameric hemoglobin from *Ascaris.* The observed changes over the entire spectrum are very similar to what was previously observed for the D1 fragment of Hb Ascaris (Huang et al., 1996). In particular, the intensity of the hydrogen bonding sensitive Y8a and Y8b tyrosine modes (at ∼1615 and 1600 cm^{-1}, respectively) increased upon binding oxygen. A very much reduced change (not shown) occurs upon the binding of CO as previously reported in the D1 fragment (Huang et al., 1996). Figure 2 shows a larger region of the UVRR

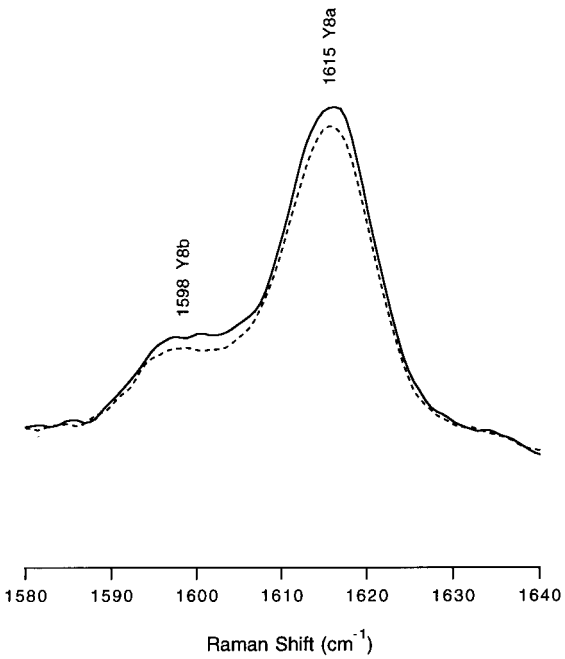

FIGURE 1: Comparison of the Y8a and Y8b regions of the 230 nm excited UV resonance Raman spectra of the oxy (solid curve) and deoxy derivatives (dashed curve) of the perienteric hemoglobin from *A. suum*.

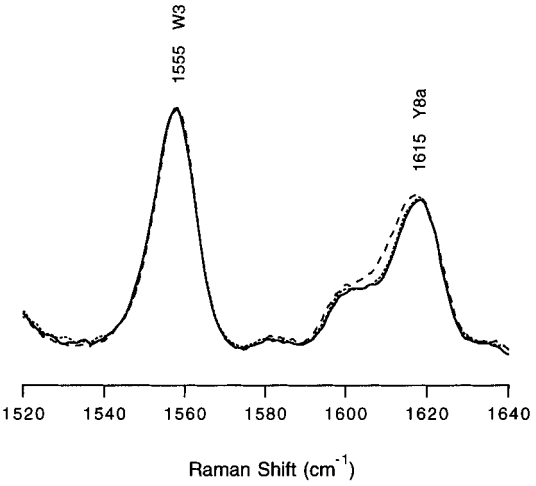

FIGURE 2: Comparison of the high-frequency region of the UV resonance Raman spectra of the oxy (solid curve), carbonmonoxy (dotted curve), and deoxy (dashed curve) derivatives of Lucina Hb-II hemoglobin.

spectrum for the deoxy, CO, and O_2 derivatives of Hb-II from *Lucina.* In contrast to Hb Ascaris, which shows a gain in the intensity of the Y8a and Y8b bands upon binding of oxygen, but not carbon monoxide, Lucina Hb-II exhibits a decrease in the intensity of these two tyrosine bands for both ligands. In addition, the deoxy derivative of Lucina Hb-II exhibits a slight shift to lower frequency for the more intense Y8a band relative to the two ligand-bound forms. No ligand-induced changes in the W3 tryptophan band at ∼1555 cm^{-1} are observed.

Visible Resonance Raman (VRR) Spectra. Figure 3 shows the low-frequency region of the Soret-enhanced VRR spectra for the photoproduct at 10 ns (henceforth referred to as Hb*) of the CO derivatives of Lucina Hb-II and Hb Ascaris (both the D1 fragment and the full perienteric octameric form). We focus primarily on the low-frequency peak occurring between 200 and 220 cm^{-1} which is assigned to the iron−

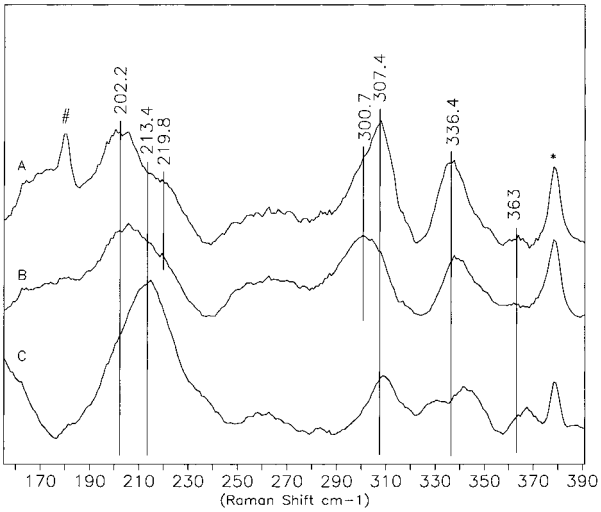

FIGURE 3: Comparison of the Soret-enhanced visible resonance Raman spectra of the CO photoproducts at 10 ns of (A) the perienteric Hb from *A. suum*, (B) the recombinant D1 fragment of Hb Ascaris, and (C) Lucina Hb-II. Within the signal-to-noise, the corresponding deoxy spectra are the same as the 10 ns photoproduct spectra. The asterisk labels a Raman band from the sapphire window of the sample cell, and the # labels a laser line from rotationally hot hydrogen within the pressure cell used to generate the 436 nm excitation. The spectra were normalized using the ν_7 mode band at 673 cm^{-1}.

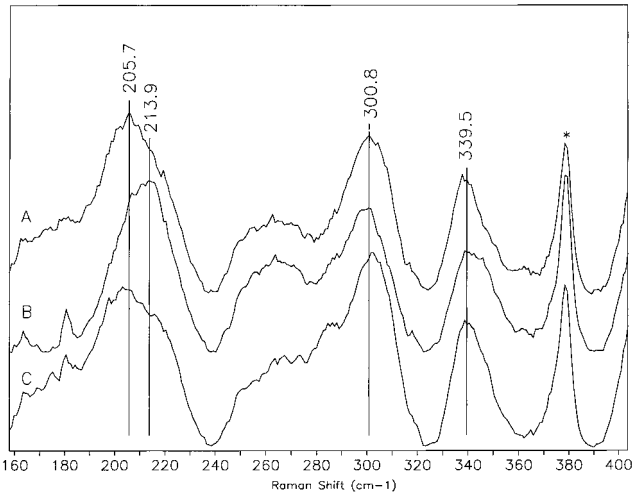

FIGURE 4: Comparison of the 10 ns $COHb^*$ photoproduct visible resonance Raman spectra of (A) the wild-type recombinant D1 fragment of Hb *A. suum*, (B) the Arg F7→Ser D1 mutant, and (C) the Arg F7→Leu D1 mutant. The asterisk indicates a sapphire window Raman line. The spectra were normalized using the ν_7 mode band at 673 cm^{-1}.

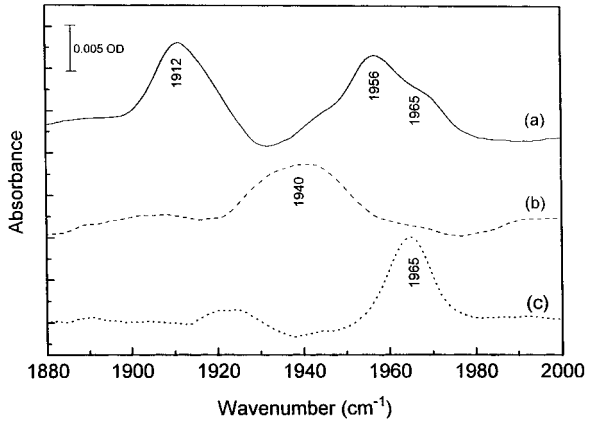

FIGURE 5: FTIR spectra of the CO derivatives of (a) the wild-type D1 fragment of Hb Ascaris, (b) the D1 B10 Tyr→Phe Hb Ascaris mutant, and (c) Lucina Hb-II.

proximal histidine stretching mode, ν(Fe−His) (Argade et al., 1984; Rousseau & Friedman, 1988; Kitagawa, 1988; Wells et al., 1991). For the *Ascaris* samples, ν(Fe−His) appears as two bands. The more intense lower frequency band is at ∼202 cm^{-1} for the octameric protein and at ∼206 cm^{-1} for the D1 fragment, respectively; however, it is difficult to be certain whether this is an actual frequency shift or just a difference in the relative contributions of subpopulations due to conformational disorder in the sample on the time scale of the experiment. The higher frequency shoulder is at ∼220 cm^{-1} in both *Ascaris* samples. A similar study using significantly more intense excitation pulses on an old sample of the octameric form that had been frozen for several years showed a similar pattern but with near equal intensity for the two bands. No obvious difference is observed between the deoxy form and the photoproduct derived from either COHb or O_2Hb (data not shown).

The Lucina Hb-II* exhibits a single broad band at ∼213 cm^{-1}. The relative intensity of ν(Fe−His) for Lucina Hb-II* compared to the Raman bands from the heme is considerably greater than for Hb Ascaris.

The Raman bands between 300 and 375 cm^{-1} are sensitive to the interactions of the heme propionates (Hu et al., 1993, 1997; Jayaraman & Spiro, 1996). In contrast to vertebrate Hbs and Mbs, neither Hb Ascaris nor Lucina Hb-II exhibits a strong band between 360 and 375 cm^{-1}. For Hb Ascaris, there is a very weak peak at ∼363 cm^{-1} and a more intense ∼336 cm^{-1} band. Lucina Hb-II has a single relatively weak band at ∼368 cm^{-1} and a doublet at 330 and 343 cm^{-1}.

Figure 4 shows the low-frequency region of the Raman spectrum of the CO photoproduct at 10 ns for the wild-type D1 fragment of Hb* Ascaris and two mutants, F7 Arg→Ser and F7 Arg→Leu. Minimal differences exist between the spectrum of the wild type and that of F7 Arg→Leu, although the mutant displays a slightly decreased frequency in the dominant component of the ν(Fe−His) band. In contrast, the spectrum for the F7 Arg→Ser mutant shows a single ν-(Fe−His) band at ∼214 cm^{-1} and a broadening of the propionate-sensitive band at 340 cm^{-1}.

FTIR. Figure 5 shows the CO stretching frequency in the ambient temperature FTIR spectra of native D1 COHb Ascaris, r COHb Ascaris B10 Tyr→Phe, and Lucina COHb-II in a 75% glycerol/water solvent. It can readily be seen that COHb Ascaris has a distinct and substantial peak at 1912 cm^{-1} as well as a broad structured peak at 1956 cm^{-1} with a shoulder at 1965 cm^{-1}. The B10 mutant has a single broad band at 1940 cm^{-1}. Lucina COHb-II exhibits a sharp band at 1965 cm^{-1} and a weak band at 1923 cm^{-1}.

Ligand Recombination. Figure 6 shows a comparison of the nanosecond geminate recombination of CO for the wild-type D1 fragment of Hb Ascaris, the E7 Gln→Leu D1 mutant, and the B10 Tyr→Phe D1 mutant. It can be seen that replacing the tyrosine with a phenylalanine reduces geminate rebinding, whereas replacing the glutamine with a leucine increases geminate rebinding. In Figure 7, the full rebinding curve (geminate rebinding on the nanosecond to microsecond time scale and solvent-derived bimolecular recombination on the slower time scale) for the CO derivatives of these Hbs is shown as a log−log plot of the survival

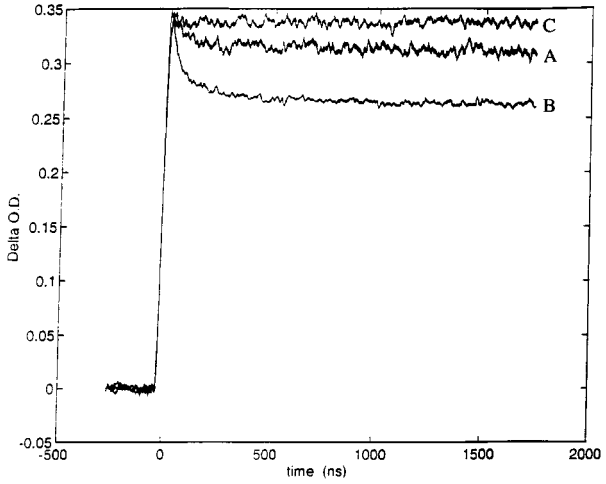

FIGURE 6: Comparison of the room temperature nanosecond geminate recombination for the CO derivatives of Hb Ascaris D1 fragments: (A) wild type, (B) E7 Gln→Leu, and (C) B10 Tyr→Phe.

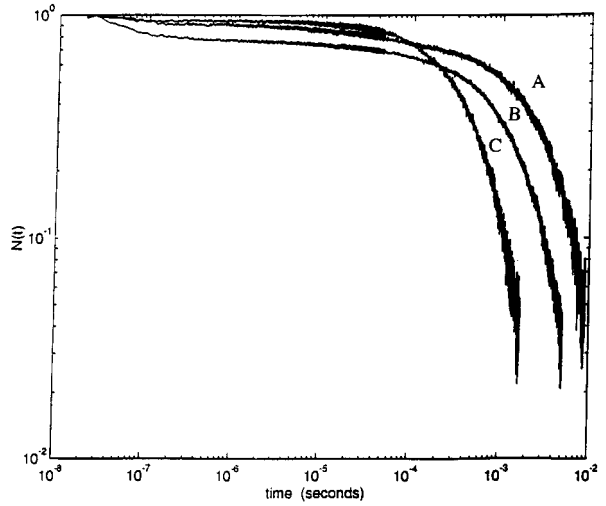

FIGURE 7: Comparison of the entire CO rebinding process (geminate plus solvent) for the three Hb Ascaris D1 fragments shown in Figure 6: (A) wild type, (B) E7 Gln→Leu, and (C) B10 Tyr→Phe. The rebinding is displayed as a log−log plot of the survival probability of the photoproduct [$N(t)$] versus time.

probability of the photoproduct versus time. Both mutations result in an acceleration of the solvent phase rebinding that takes place on the millisecond time scale. The B10 Try→Phe mutation produces the greater increase in rate.

Figure 8 shows the effect of a modest decrease in temperature (292→280 K) upon the ligand rebinding to photodissociated COHb Ascaris (WT octamer) in aqueous buffer. It can be seen that the decrease in temperature results in a substantial increase in geminate rebinding and a decrease in the solvent phase. In contrast, it can be seen in Figure 9 that for Lucina COHb-II there is no discernible nanosecond geminate phase at either 292 or 280 K. The solvent phase for the recombination of CO to Lucina Hb-II does show a rate decrease with the decrease in temperature (not shown).

The comparison of the nanosecond geminate rebinding of oxygen to Lucina Hb-II, HbA (human adult hemoglobin), and Hb Ascaris (octamer) is shown in Figure 10. All three samples were of near equal heme concentration. Lucina Hb-II shows no geminate rebinding and has the largest amplitude at 10 ns for the creation of photoproduct. HbA has a lower amplitude at 10 ns and exhibits the previously observed

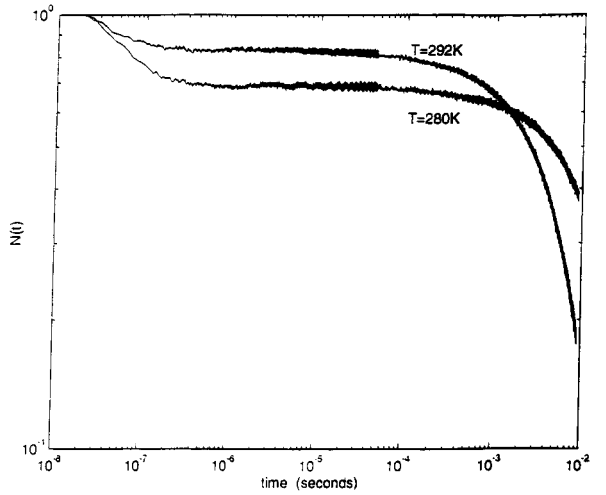

FIGURE 8: Temperature dependence at 280 and 292 K of the geminate and solvent phase CO recombination for the native perienteric Hb from *A. suum*.

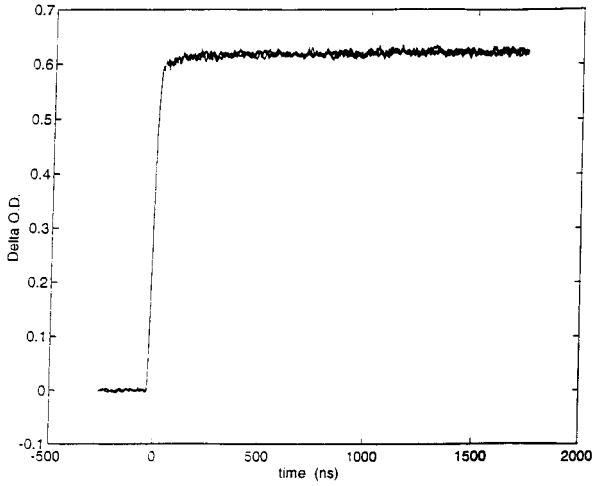

FIGURE 9: Temperature dependence at 280 and 292 K of the CO recombination for Lucina Hb-II on the nanosecond to microsecond time scale.

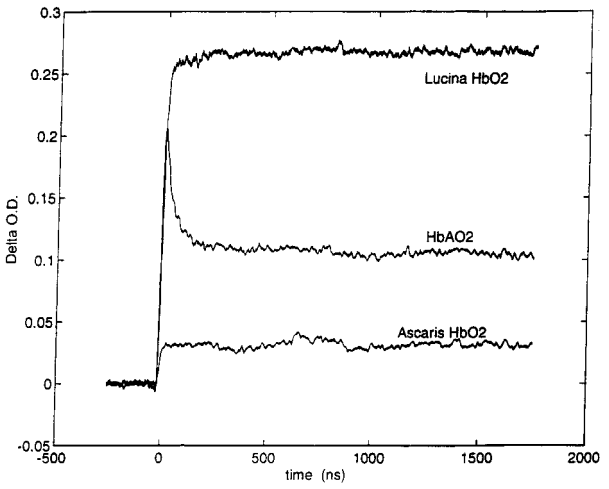

FIGURE 10: Comparison of the nanosecond oxygen geminate rebinding and photolysis yield (at 10 ns) at 292 K for Lucina Hb-II, human adult Hb (HbA), and Hb Ascaris. The samples were all at the same heme concentration, and the laser power was adjusted for maximum photolysis.

(Scott & Friedman, 1984) nanosecond geminate phase. Hb Ascaris has a very low initial amplitude and also appears to display no geminate rebinding.

DISCUSSION

Despite the fact that Hb Ascaris and Lucina Hb-II both have the same unusual E7 and B10 residues, they exhibit substantial differences in many aspects of structure and function. In the following discussion, the two proteins are compared with respect to ligand reactivity and local structure at the heme. The spectroscopic and kinetic studies presented herein suggest details of how aspects of the local structure in both proteins modulate ligand binding.

Distal Heme Pocket Interactions. The UV resonance Raman spectra of the deoxy and liganded (CO and O_2) derivatives of the native form of Hb Ascaris (octamer) are very similar to what was reported earlier for the corresponding derivatives of the D1 fragment (Huang et al., 1996). In particular, we focus upon the pair of tyrosine bands, Y8a and Y8b, at ∼1615 and 1600 cm^{-1}, respectively. Based on the sensitivity of the Y8a and Y8b modes to changes in hydrogen bonding of the phenolic oxygen (Austin et al., 1993; Rodgers et al., 1992; Hildebrandt et al., 1988; Fodor et al., 1986), the present results indicate that the native form exhibits a spectral pattern consistent with the B10 Tyr contributing a proton in the formation of a hydrogen bond with the bound oxygen, but much less so with CO. A change from a non-hydrogen bonding situation to one in which the tyrosine becomes a strong proton donor should increase the cross section for Raman scattering by a factor of 2 for a 230 nm excitation (Rodgers et al., 1992). The observed change in the Raman intensity of Y8a and Y8b is less than a factor of 2 since the band also has contributions from the other tyrosines in the protein.

The FTIR spectrum of COHb Ascaris contains a prominent CO stretching band at 1912 cm^{-1}. This frequency is at the extreme lower end of the known values for CO bound to heme in both native and mutant forms of Mbs (Li et al., 1994). Analysis of the origin of the variation in CO stretching frequencies has led to the conclusion that the determining factor is the electrostatic environment of the CO and not the Fe−CO angle (Li et al., 1994; Stavrov, 1996, 1997). A value of 1912 cm^{-1} is consistent with the presence of a positive charge in very close proximity to the bound CO, and the obvious candidate for the source of this charge is the phenolic proton from the B10 Tyr based on its proximity to the bound oxygen in the X-ray structure (Yang et al., 1995). This assignment is supported by the finding that the B10 Tyr→Phe mutant does not exhibit this same low-frequency component. Furthermore, the appearance of additional high-frequency CO stretching bands at 1956 and 1965 cm^{-1} in the FTIR spectrum of COHb Ascaris suggests that at room temperature conformations also exist in which the B10 residue is not in close proximity to the bound ligand.

The 1940 cm^{-1} frequency observed for the B10 Tyr→Phe mutant is higher than the frequency of 1932 cm^{-1} for the corresponding mutant in mammalian Mb, which has been interpreted as arising from the close proximity of the positive multipole of the B10 phenyl ring (Li et al., 1994; Balasubramanian et al., 1993). The higher frequency observed for Hb Ascaris suggests that the phenyl ring is not as close as in the mammalian case. In fact, the 1940 cm^{-1} frequency is closer to the frequency that is observed for the E7 His→Gln mammalian Mb mutant (1945 cm^{-1}) (Li et al., 1994). These observations imply that in the B10 Tyr→Phe Hb Ascaris mutant, it is the glutamine at position E7 (and possibly any nearby water molecules) that determines the electrostatic field on the bound CO and that the loss of the hydrogen bonding capabilities of the tyrosine side chain upon mutation to a B10 phenylalanine results in a movement of the B10 phenyl ring away from the bound CO.

The UV resonance Raman spectra of the different derivatives of Lucina Hb-II reveal a very different pattern from what is observed for Hb Ascaris. For both the CO and O_2 derivatives of Lucina Hb-II, the Y8a and Y8b bands decrease in intensity and shift slightly to higher frequency compared to the corresponding deoxy values. Based on the correlation between spectral parameters associated with these two tyrosine Raman bands and the hydrogen bonding properties of the tyrosine noted above, it appears that ligand binding to Lucina Hb-II results in the formation of a hydrogen bond in which tyrosine is a proton acceptor, rather than a proton donor as occurs in the oxy derivative of Hb Ascaris.

The FTIR spectrum of Lucina COHb-II lacks the pronounced 1912 cm^{-1} band seen in COHb Ascaris, which suggests that the phenolic proton from the B10 Tyr is not as close to the bound CO in Lucina Hb-II as it is in Hb Ascaris. However, the presence of the low-frequency 1923 cm^{-1} band in the Lucina COHb-II spectrum indicates that the bound CO does have more positive charge near it than is typical for Mbs with either histidine or glutamine as the E7 residue (Li et al., 1994). The high-frequency peak at 1965 cm^{-1} is consistent with there being an absence of positive charge influencing the bound CO in part of the population. It is noteworthy that in the mammalian Mb system none of the B10 mutations result in a CO band with this high frequency, but that the replacement of His E7 with tyrosine does produce an environment that gives rise to a similar frequency. It thus appears that if the tyrosine is oriented and localized appropriately, it can shift the bound CO frequency up to 1965 cm^{-1}. Obviously, this positioning of the tyrosine must be substantially different than that which gives rise to the very low frequency observed for COHb Ascaris (1912 cm^{-1}).

Proximal Heme Pocket Interactions. As noted above, the low-frequency portions of the Soret-enhanced resonance Raman spectra of deoxy hemoglobins contain two classes of very important bands. In the region between ∼200 and 230 cm^{-1} is ν(Fe−His), the iron−proximal histidine stretching mode. Between 300 and 375 cm^{-1} are several bands whose frequencies are sensitive to the interactions between the heme propionates and surrounding residues and solvent.

The frequency of ν(Fe−His) is determined by several factors, the most significant of which is the F helix modulated tilt of the proximal imidazole with respect to the heme plane. Upon ligand dissociation, the F helix shifts away from the FG corner toward the EF corner (in the typical myoglobin fold) and a causes a corresponding increase in the tightly coupled imidazole tilt angle that then results in an enhanced steric repulsion between the pyrrole nitrogens and the nearest imidazole carbons (Gelin & Karplus, 1977). This enhanced repulsion results in a decrease in the frequency of the ν(Fe−His) mode, most likely by increasing the displacement of the iron (Stavrov, 1993), and makes it energetically more costly to move the iron in-plane upon ligand binding (Friedman et al., 1982; Rousseau & Friedman 1988; Friedman, 1985, 1994; Šrajer et al., 1988). These structural changes and the barrier increase are collectively referred to as "proximal strain". Changes in the tilt angle with change in both quaternary and tertiary structure are the likely origin

of how ligand binding affinity is modulated in vertebrate hemoglobins. Geminate recombination, ligand on rates, and overall ligand binding affinities are responsive to these changes (vide infra) (Matsukawa et al., 1984; Friedman et al., 1985; Perutz et al., 1987; Rousseau & Friedman, 1988; Perutz, 1989; Friedman, 1994).

The X-ray structure of the oxy derivative of Hb Ascaris shows that the proximal histidine in this protein is indeed tilted (Yang et al., 1995). Since no X-ray structures have been solved for the deoxy derivative of Hb Ascaris or any derivative of Lucina Hb-II, it is not yet known if the F helix, and therefore also the imidazole tilt, changes upon ligation. In addition, the ν(Fe−His) band does not appear in the Raman spectrum of the 6-coordinate species, so it also cannot be used to determine if these changes have occurred. However, the identical appearance of the Raman spectra of the CO photoproduct at 10 ns and the deoxy derivatives for both Hb Ascaris and Lucina Hb-II strongly suggests that in these proteins there is minimal change in the F helix position and the degree of imidazole tilt upon ligation since it is unlikely that a significant movement of the F helix could occur within 10 ns. This is consistent with the changes seen in human HbA, where the F helix movement only occurs after several tens of nanoseconds and continues into the microsecond regime (Scott & Friedman, 1984; Jayaraman et al., 1995; Jayaraman & Spiro, 1996).

The azimuthal angle of the proximal imidazole ring is another degree of freedom that can contribute to proximal strain (Ahmed et al., 1991). In the eclipsed orientation, the imidazole carbons lie above the pyrrole nitrogens, which, as explained above, enhances steric repulsion between the heme and the imidazole and makes it energetically more costly to bind a ligand. In contrast to the histidine tilt, which appears to be modulated by shifts of the F helix relative to the heme, the azimuthal angle of the proximal imidazole appears to be primarily controlled by a more local interaction, most likely involving hydrogen bonding between the $N_\delta H$ of the imidazole and adjacent residues on the F helix. For example, hydrogen bonds to the $N_\delta H$ from the hydroxyl of the F7 Ser and the backbone carbonyl of residue F4 (usually leucine) are thought to be responsible for the near-eclipsed imidazole orientation in vertebrate myoglobins (Smerdon et al., 1993).

The proximal histidine tilt, the azimuthal angle of the proximal imidazole, and the iron displacement are expected to be highly coupled (Ahmed et al., 1991; Friedman, 1994). For example, a large tilt angle should greatly increase the steric consequences of an eclipsed imidazole orientation. The extent to which the protein can adopt an energetically more favorable conformation is a factor in the control of its reactivity. For instance, X-ray crystallographic studies of lupin leghemoglobin show that the proximal imidazole assumes two different partially eclipsing azimuthal orientations in the deoxy state but adopts a single staggered and less tilted orientation upon oxygen binding (Harutyunyan et al., 1995).

Analyses of the response of ν(Fe−His) to changes in the azimuthal angle are complicated by the fact that as the hydrogen bonding to the N_δ of the proximal imidazole decreases so does the frequency (Spiro et al., 1990), possibly due to modulation of the electron density at the N_ϵ by the $N_\delta H$ hydrogen bond strength (Peisach & Mims, 1977; Valentine et al., 1979). Thus, a reduction in the hydrogen bonding that also results in a more staggered azimuthal angle could result in opposing shifts in the frequency of ν(Fe−His).

The low-frequency Soret band enhanced resonance Raman spectra of Hb Ascaris reveal what appears to be a doublet for ν(Fe−His) (Figure 3). The main peak occurs at ∼204 cm^{-1}, and a shoulder appears at ∼220 cm^{-1} for both domain 1 and the intact octamer, although the relative intensities of the two bands are slightly different for the two samples. An earlier set of data derived from the intact native protein, but taken at a higher temperature with much higher pulse energies, also displayed the same two peaks, but with the 220 cm^{-1} band much more pronounced. The power dependence of these results suggests that a temperature-dependent shift between at least two conformations might be occurring. The extreme low frequency of the main component corresponds to a population in a conformation with significant proximal strain and with the N_δ proton at most weakly hydrogen bonded. The low ν(Fe−His) frequency observed in the deoxy derivative of the dimeric hemoglobin from *Scapharca inaequivalis* has been explained by a similar structure (Rousseau et al., 1993). A plausible explanation for the high-frequency band is that it corresponds to another population that does have a hydrogen bonded imidazole N_δ proton.

The role of hydrogen bonding in stabilizing these possible proximal imidazole conformations is strongly supported from the spectrum of the F7 Arg→Ser mutant which shows the collapse of the two peaks into one distinct band (Figure 4). In contrast, the spectrum of the F7 Arg→Leu mutant does not show this collapse. Serine in position F7 is known to form a hydrogen bond to the N_δ of the proximal histidine, whereas leucine would not (Shiro et al., 1994; Smerdon et al., 1993). Hence, it is reasonable to ascribe the collapse of the two bands into one as being the result of the serine stabilizing a particular azimuthal angle through the formation of a hydrogen bond to the proximal histidine. The resulting frequency for the single ν(Fe−His) is still quite low at ∼213 cm^{-1} (vis-à-vis ∼220 cm^{-1} for Mb and ∼213 cm^{-1} for deoxy T state HbA), indicative of considerable proximal strain, as is the case in the T state of HbA.

Preliminary X-ray crystallographic studies (F. S. Mathews, private communication) on the oxy derivatives of WT and the F7 Arg→Ser, Leu mutants of the D1 fragment reveal no variation in the azimuthal angle. This suggests a situation analogous to the leghemoglobin in which ligand binding locks in a single rotational conformation of the proximal histidine (Harutyunyan et al., 1995). Again, since the ν-(Fe−His) band does not appear in the Raman spectra of the six-coordinate derivatives, a direct test of this hypothesis using Raman is not possible. However, the CO photoproduct results, which show that the Hb* spectrum at 10 ns is identical to that of the deoxy derivative, imply that in all the Hb Ascaris samples except the F7 serine mutant the photodissociation of the ligand results in a very rapid relaxation of the histidine to the two-conformer situation observed in the deoxy derivative. It is known (Findson et al., 1985) that for mammalian Mbs, the relaxation of the proximal environment subsequent to photodissociation is significantly faster than the 10 ns resolution in the present study. Confirmation of this proposed scenario requires added X-ray or NMR studies on the deoxy species to better establish the existence of the two populations as well as cryogenic or

picosecond photodissociation studies in an attempt to trap the photoproduct in a single rotational conformer of the proximal histidine.

The ν(Fe−His) for the 10 ns photoproduct of Lucina COHb-II appears as a single intense band at ∼213 cm^{-1}. Compared to Hb Ascaris, it has a much greater relative intensity with respect to the Raman bands derived from the heme modes. Based on the admittedly uncertain relationship between azimuthal angle and resonance enhancement for ν-(Fe−His) [i.g., the ν(Fe−His) band intensity] (Friedman et al., 1990; Ahmed et al., 1991), we tentatively attribute the low frequency and the high intensity of ν(Fe−His) to a highly eclipsed orientation for the proximal histidine in conjunction with significant proximal strain. An alternative possibility is that the intensity is being modulated by the local dielectric field of the heme pocket.

Geminate and Solvent Recombination of Photodissociated Ligands. The rebinding studies on Lucina Hb-II are indicative of efficient ligand escape from the heme pocket for both CO and O_2 subsequent to photodissociation. This result is consistent with a relatively high inner barrier controlling ligand−iron bond re-formation and minimal constraints to ligand escape. The high inner barrier is further in evidence from the slow bimolecular rebinding of oxygen compared to the same process in HbA (not shown). Since there is no indication of protein constraints on the diffusion of ligands through the protein to or away from the heme (as reflected in the ease of ligand escape upon photodissociation), the slow rebinding is ascribed to a high inner barrier, not to a barrier to or from the solvent. The low frequency of the ν(Fe−His) band suggests that the presence of proximal strain contributes to the barrier being high. Alternatively, the low bimolecular on rate could also arise from distal effects if the distal heme pocket of deoxy Lucina Hb-II contains a population of waters that need to be displaced prior to ligand binding. Furthermore, if the distal pocket is readily accessible to water, it may be the case that the low geminate yield upon ligand photodissociation is due to successful competition by water for the volume of the distal pocket. However, it is unlikely that a population of mobile waters resides in the distal pocket when the ligand is bound to the heme since the CO stretching frequencies and line shapes are completely different from those of Mb mutants that are known to have waters in the distal pocket (e.g., His64→Gly) (Li et al., 1994). This conclusion does not preclude the possibility of an ordered water bound in a highly specific fashion within the distal pocket of Lucina Hb-II (vide infra).

In contrast to Lucina Hb-II, which shows no indication of geminate recombination, Hb Ascaris exhibits a substantial geminate yield for O_2 and a moderate yield for CO. It can be seen that relative to HbA and Lucina Hb-II, the effective quantum yield for the photodissociation at 10 ns of O_2Hb Ascaris is drastically reduced (Figure 10), suggesting the presence of a very efficient subnanosecond geminate phase. Earlier studies provide indications of a picosecond geminate phase (Gibson et al., 1993). More recently, preliminary studies by Ridsdale and Pereira (unpublished) using low-energy femtosecond pulses suggest that all but a few percent of the photodissociated oxygen is rebound within ∼5 ps. This finding implies that the somewhat larger (∼14%) quantum yield for O_2 photodissociation shown in Figure 10 is probably the result of a buildup of photoproduct due to continued rephotolysis over the duration of the 10 ns pulse and that the apparent lack of a nanosecond geminate phase is due to an efficient escape pathway for those oxygens that do not undergo the picosecond rebinding.

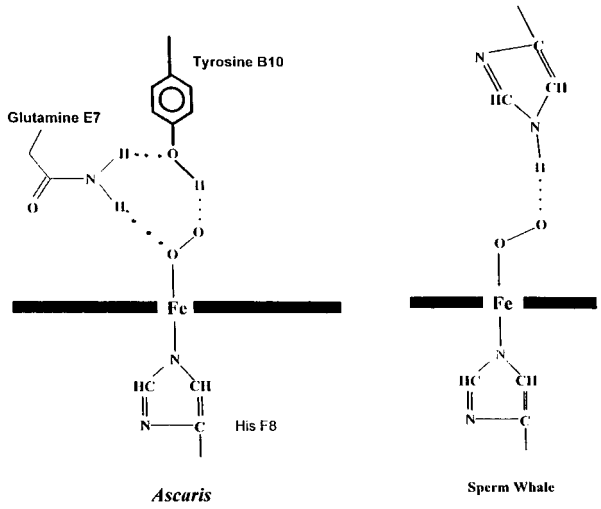

FIGURE 11: Schematic comparing the proposed hydrogen bonding pattern within the distal pocket in Hb Ascaris to that of sperm whale myoglobin.

All of the results and conclusions discussed above now allow us to propose a model invoking two possible distal hydrogen bonding networks involving the oxygen ligand and an ordered water molecule to account for the differences in affinity seen in Hb Ascaris and Lucina Hb-II in spite of their both having the same B10 Tyr and E7 Gln motif.

We suggest that in Hb Ascaris the equilibrium structure has a cage-like distal pocket that does not allow ligand motion away from the heme after photodissociation and may constrain the O_2 so as to facilitate rebinding in a zero barrier process on a picosecond or faster time scale before the iron moves significantly out of plane, thus giving rise to the high geminate yield. A similar argument was used to explain the presence of a nonphotolyzable population of O_2 HbA at 4 K (Chance et al., 1990). Alternatively, the presence of the B10 tyrosine may stabilize the transition state for rebinding either electrostatically or sterically, effectively lowering the barrier. An interesting possibility for steric modulation may arise if the oxygen remains transiently tethered to the B10 tyrosine via a hydrogen bond subsequent to photodissociation.

The above cage model is supported by previous X-ray crystallographic (Yang et al., 1995) and UV Raman data (Huang et al., 1996) that both indicate that the B10 Tyr, E7 Gln, and ligand can form a hydrogen bonding network, schematically depicted in Figure 11. The schematic for Mb is shown for comparison. In addition to the data presented herein, an additional example of the extreme tightness of the cage is reflected dramatically in the inability to substantially photodissociate O_2Hb Ascaris at 10 K ($Q_Y \leq 0.10$) with continuous illumination under conditions that result in a quantum yield of 0.5 for O_2Mb (Miller et al., 1996) and 0.35 for Lucina O_2Hb-II.

The FTIR results indicate that the Hb Ascaris distal pocket can assume multiple conformations. For the bound oxygen complex, it is likely that the strong hydrogen bonding network favors a closed conformation as seen in the crystallographic data (Yang et al., 1995). Periodic thermal fluctuations could then result in opening of the distal pocket, and if photodissociation occurs close in time to such a

fluctuation, ligand escape could occur with a greatly enhanced probability. The small population of nonrebinding photoproduct seen on the nanosecond time scale for O_2Hb Ascaris would represent the fraction of molecules that underwent this opening of the distal pocket coincident with the excitation pulse. Once outside the pocket, the ligand would have a low probability of rebinding after the tightly closed distal cage had re-formed. The very slow solvent phase rebinding is also consistent with a restricted access to the heme.

Replacement of the B10 Tyr with Phe in Hb Ascaris results in a decrease in the geminate yield for CO and an increase in the rate of the solvent phase, consistent with a disruption of the distal pocket cage. There is evidence that the presence of a B10 Phe in Mb enhances geminate rebinding at early times by blocking escape, but limits geminate rebinding for those ligands that have diffused beyond the B10 side chain (Gibson et al., 1992). The FTIR results on the CO derivative of the B10 Tyr→Phe mutant of Hb Ascaris indicate that the phenyl ring is not as close to the CO as in the corresponding Mb mutant (vide supra) and therefore does not provide the same ligand diffusion constraints as in Mb. Thus, the disruption of the distal cage via the B10 Tyr→Phe replacement in Hb Ascaris probably allows the ligand to rapidly diffuse beyond B10, and this is probably also the case in Lucina Hb-II (vide infra). In addition, the presence of the polar E7 Gln and the open pocket should favor the introduction of water into the pocket after the ligand escapes, which would have the effect of slowing the rebinding of a ligand that has diffused outside of the pocket.

The replacement of E7 Gln with a Leu enhances both the geminate phase and the rate of the solvent phase rebinding for CO. It is likely that this substitution leads both to a partial disruption of the distal cage through the loss of the E7−B10 hydrogen bond (vide infra) and to a more hydrophobic environment in the distal pocket. These changes are likely to enhance the solvent phase ligand rebinding by enhancing access to the heme and by making it easier to displace any competing water molecules. The increased geminate yield for CO in spite of a partial disruption of the caged pocket could be the result of several factors, including the formation of a new docking site within the distal pocket, the reduction in steric hindrance, or a greater pocket occupancy factor for the dissociated ligand due to less competition from water.

The substantial increase in the geminate yield for COHb Ascaris, in going from 292 to 280 K, can be explained in terms of the temperature dependence of the distal pocket cage. Transient disruption of this network leading to ligand escape is likely to require a large-amplitude thermal fluctuation of the globin. Such large motions can be expected to have a large activation energy and thus be highly sensitive to modest temperature or viscosity changes at ambient temperatures.

The conclusion that ligand escape for Hb Ascaris is only possible when the protein undergoes a transient opening of the distal cage raises the question of how oxygen can ever escape once bound. The answer is that the same fluctuations that open the pocket also disrupt the hydrogen bonds to the oxygen. Once this loss of the hydrogen bond occurs, the oxygen has a much higher probability for dissociation, especially because of the unfavorable proximal environment [high proximal strain as reflected in ν(Fe−His)]. Since

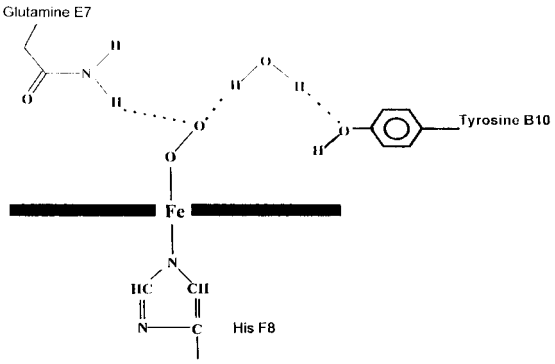

FIGURE 12: Schematic of the proposed hydrogen bonding pattern for the distal heme pocket in Lucina Hb-II hemoglobin.

dissociation is highly coupled with the opening of the pocket, a ligand spontaneously dissociated in this way has a high probability for escape (again, the poor proximal environment, the loss of the distal hydrogen bonding, and the open distal pocket all favor escape over rebinding). In contrast, in the photodissociation experiments, the ligand is dissociated in a manner that is only rarely coincident with the transient opening of the pocket, and as a result a nonphysiological situation is created in which there is a dissociated ligand in a tight and closed distal pocket, and geminate rebinding is assured. For CO, the situation is modified by virtue of the inherently looser distal cage due to the much weaker hydrogen bond between the distal pocket residues and the bound CO. As a result, a dissociated CO is more likely to be situated in an open or looser distal pocket than is a dissociated oxygen.

The situation for *Lucina* is clearly different. Ligand escape and entry into the distal pocket are not restricted. The UV Raman data indicate that the B10 Tyr is not providing a stabilizing proton to the bound oxygen. Nonetheless, Lucina O_2Hb-II has a very low spontaneous ligand off rate (Kraus & Wittenberg, 1990). A schematic of a possible structure that can account for these findings is shown in Figure 12. The distal pocket is assumed to be relatively open. If we assume that water can occupy the distal pocket at the same time as bound oxygen, we can have water forming a bridge between the phenolic oxygen of the B10 Tyr and the bound oxygen. This structure accounts for the UV Raman spectra in that the binding of a ligand results in the formation of a conformation in which the tyrosine accepts a proton upon ligand binding. The hydrogen bond to the bound ligand from the ordered water molecule would then account for the reduced off rate for O_2. Upon dissociation, ligand escape is favored as a result of the rapid collapse of the bridging structure, the diffusion of this water molecule, the unfavorable proximal conformation, and the open distal pocket. The relatively low frequency for one of the CO stretching bands observed for Lucina COHb-II is consistent with the proton of the ordered water being hydrogen bonded to the bound CO. Alternatively, the B10 tyrosine in *Lucina* may be sufficiently mobile that upon ligand binding it can assume an orientation that results in an altered interaction between the multipole charge distribution of the ring and the bound ligand which then produces the UV resonance Raman changes.

CONCLUSIONS

Despite the presence of the same B10 and E7 residues, the hemoglobins from *Ascaris* and *Lucina* display dramati-

cally different oxygen affinities and mechanisms for achieving their respective functionality. Hb Ascaris has a distal heme pocket that provides a very tight and nearly inescapable cage for the heme-bound ligand. The B10 tyrosine directly interacts with the bound ligand through the phenolic proton. Ligand dissociation within this tight pocket, such as occurs in photolysis, results in rapid rebinding. There is evidence, however, that the protein can also adopt alternate, though infrequent, conformations in which the distal pocket is open, resulting in a destabilization of the bound ligand and an enhanced rate of escape for a dissociated ligand. Thus, large-amplitude fluctuations of the distal heme pocket in conjunction with high proximal strain favor ligand dissociation under conditions where ligand escape is also maximized. It is likely that a similar but less exaggerated thermally driven mechanism is at work in the spontaneous dissociation of O_2 from vertebrate Mbs and Hbs. In those cases, fluctuations involving the distal histidine simultaneously weaken the iron−oxygen bond and provide an enhanced escape route for the dissociated ligand.

In Lucina Hb-II, the distal pocket is much more open than in Hb Ascaris, allowing for rapid escape of a dissociated ligand. A novel structure is proposed for ligand-bound Lucina Hb-II that accounts for the observed spectroscopy and ligand kinetics in which a water forms a bridging structure between the bound ligand and the phenolic oxygen of Tyr B10. Together, the two proteins demonstrate both the extraordinary plasticity of the myoglobin fold and the subtle interplay among structure, dynamics, sequence, and functionality.

ACKNOWLEDGMENT

We thank Drs. F. Scott Mathews, A. Ridsdale, and M. Pereira for allowing us to cite preliminary unpublished results.

REFERENCES

Ahmed, A. M., Campbell, B. F., Caruso, D., Chance, M. R., Chavez, M. D., Courtney, S. H., Friedman, J. M., Iben, I. E. T., Ondrias, M. R., & Yang M. (1991) *Chem. Phys. 158*, 329−351.

Alpert, B., Mohsni, E., Lindqvist, J., & Tfibel, F. (1979) *Chem. Phys. Lett. 64*, 11−16.

Antonini, E., & Brunori, M. (1971) in *Hemoglobins and Myoglobins in their Reactions with Ligands*, Am Elsevier Co., New York.

Argade, P. V., Sassaroli, M., Rousseau, D. L., Inubushi, T., Ikeda-Saito, M., & Lapidot, A. (1984) *J. Am. Chem. Soc. 106*, 6593−6596.

Asher, S. (1993) *Anal. Chem. 65*, 59−65.

Asher, S. A., Johnson, C. R., & Murtaugh, J. (1983) *Rev. Sci. Instrum. 54*, 1657.

Austin, J. C., Rodgers, K. R., & Spiro, T. G. (1993) *Methods Enzymol. 226*, 374-396.

Balasubramanian, S., Lambright, D. G., Marden, M. C., & Boxer, S. G. (1993) *Biochemistry 32*, 2202−2212.

Braunstein, D., Ansari, A., Berendzen, J., Cowen, B. R., Egeberg, K. D., Frauenfelder, H., Hong, M. K., Ormos, P., Sauke, T. B., Scholl, R., Schulte, A., Sligar, S. G., Springer, B. A., Steinback, P. J., & Young, R. D. (1988) *Proc. Natl. Acad. Sci. U.S.A. 85*, 8497−8501.

Carlson, M. L., Regan, R., Elber, R., Li, H., Phillips, G. N., Jr., Olson, J. S., & Gibson, Q. H. (1994) *Biochemistry 33*, 10597−10606.

Carver, T. E., Brantley, R. E., Jr., Singleton, E. W., Arduini, R. M., Quillin, M. L., Phillips, G. N., Jr., & Olson, J. S. (1992) *J. Biol. Chem. 267*, 14443−14450.

Chance, M. R., Courtney, S. H., Chavez, M. D., Ondrias, M. R., & Friedman, J. M. (1990) *Biochemistry 29*, 5537−5545.

Davenport, H. E. (1949) *Proc. R. Soc. London, Ser. B 136*, 225−270.

De Baere, I., Liu, L., Moens, L., Van Beeumen, J. V., Gielens, C., Richelle, J., Trotman, C., Finch, J., Gerstein, M., & Perutz, M. (1992) *Proc. Natl. Acad. Sci. U.S.A. 89*, 4638-4642.

De Baere, I., Perutz, M., Kiger, L., Marden, M. C., & Poyart, C. (1994*) Proc. Natl. Acad. Sci. U.S.A. 91*, 1594−1597.

Duddell, D. A., Morris, R. J., & Richards, J. T. (1979) *J. Chem. Soc., Chem. Commun.*, 75−76.

Findsen, E. W., Scott, T. W., Chance, M. R., Friedman, J. M., & Ondrias, M. R. (1985) *J. Am. Chem. Soc. 107*, 3355−3357.

Fodor, S. P. A., Rava, R., Copeland, R. A., & Spiro, T. G. (1986*) J. Raman Spectrosc. 17*, 471.

Friedman, J. M. (1985) *Science 228*, 1273−1280.

Friedman, J. M. (1994) *Methods Enzymol. 232*, 205−231.

Friedman, J. M. & Lyons, K. B. (1980) *Nature 284*,570−572.

Friedman, J. M., Rousseau, D. L., Ondrias, M. R., & Stepnoski, R. A. (1982) *Science 218*, 1244−1246.

Friedman, J. M., Scott, T. W., Fisanick, G. J., Simon, S. R., Findsen, E. W., Ondrias, M. R., & MacDonald, V. W. (1985) *Science 229*, 187−190.

Friedman, J. M., Campbell, B. F., & Noble, R. W. (1990) *Biophys. Chem. 37*, 43−59.

Gelin, B. R., & Karplus, M. (1977) *Proc. Natl. Acad. Sci. U.S.A. 74*, 801−805.

Gibson, Q. H., Regan, R., Elber, R., Olson, J. S., & Carver, T. E. (1992) *J. Biol. Chem. 267*, 22022−22034.

Gibson, Q. H., Regan, R., Olson, J. S., Carver, T. E., Dixon, B., Pohajdak, B., Sharma, P. K., & Vinogradov, S. N. (1993) *J. Biol. Chem. 268*, 16993-16998.

Harutyunyan, E. H., Safonova, T. N., Kuranova, I. P., Popov, A. N., Teplyakov, A. V., Obmolova, G. V., Rusakov, A. A., Vainshtein, B. K., Dodson, G. G., Wilson, J. C., & Perutz, M. F. (1995) *J. Mol. Biol 251*, 104−115.

Hildebrandt, P. G., Copleand, R. A., Spiro, T. G., Otlewski, J., Laskowski, M., Jr, & Prendergast, F. G. (1988) *Biochemistry 27*, 5426.

Hockenhull-Johnson, J. D., Stern, M. S., Martin, P., Dass, C., Desidero, D. M., Wittenberg, J. B., Vinogradov, S. N., & Walz, D. A. (1991) *J. Protein Chem. 10*, 609−622.

Hu, S., Morris, I. K., Singh, J. P., Smith, K. M., & Spiro, T. G. (1993) *J. Am. Chem. Soc. 115*, 12446−12458.

Hu, S., Smith, K. M., & Spiro, T. G. (1997) *J. Am. Chem. Soc*. (in press).

Huang, S., Huang, J., Klock, A. P., Goldberg, D. E., & Friedman, J. M. (1996) *J. Biol. Chem. 271*, 958−962.

Jayaraman, V., & Spiro, T. G. (1996) *Biospectroscopy 2*, 311−316.

Jayaraman, V., Rodgers, K. R., Mukerji, I., & Spiro, T. G. (1995) *Science 269*, 1843−1848.

Johnson, C. R., Ludwig, M., O'Donnell, S., & Asher, S. A. (1984*) J. Am. Chem. Soc. 106*, 5008.

Johnson, C. R., Ludwig, M., & Asher, S. A. (1986) *J. Am.Chem. Soc. 108*, 905.

Kitagawa, T. (1988) in *Biological Application of Raman Spectroscopy* (Spiro, T. G., Ed.) Vol. III, pp 97−131, Wiley and Sons, New York.

Kitagawa, T. (1992) *Prog. Biophys. Mol. Biol. 58*, 1−18.

Kloek, A. P., Yang, J., Mathews, F. S., & Goldberg, D. (1993) *J. Biol. Chem. 268*, 17669-17671.

Kloek, A. P., Yang, J., Mathews, F. S., Frieden, C., & Goldberg, D. E. (1994)
J. Biol. Chem. 269, 2377-2379.

Kraus, D. W., & Wittenberg, J. B. (1990) *J. Biol. Chem. 265*, 1604−16053.

Kraus, D. W., & Wittenberg, J. B., Lu., J. F., & Peisach, J. (1990*) J. Biol. Chem. 265*, 16054−16059.

Li, T., Quillin, L., Phillips, G. N., Jr., & Olson, J. S. (1994) *Biochemistry 33*,1 433−1446.

Matsukawa, S., Mawatari, K., Yoneyama, Y., & Kitagawa, T. (1984) *J. Am. Chem. Soc. 107*, 1108−1116.

Miller, L. M., Patel, M., & Chance, M. R. (1996) *J. Am. Chem. Soc. 118*, 4511−4517.

Nagai, K., Luisi, B., Shih, D., Miyazaki, G., Imai, K., Poyart, C., De Young, A., Kwiatkowsky, L., Noble, R. W., Lin, S. H., & Yu, N. T. (1987) *Nature 329*, 858−860.

Okazaki, T., & Wittenberg, J. B. (1965) *Biochim. Biophys. Acta. 111*, 503−511.
Peisach, J., & Mims, W. B. (1977) *Biochemistry 16*, 2795−2799.
Perutz, M. F. (1989) *Q. Rev. Biophys. 22*, 139−236.
Perutz, M. F., Fermi, G., Luisi, B., Shaanan, B., & Liddington, R. C. (1987) *Acc. Chem. Res. 20*, 309.
Perutz, M. F., Staden, R., Moens, L., & De Baere, I. (1993) *Curr. Biol. 3*, 249−251.
Phillips, S. E. V., & Schoenborn, B. P. (1981) *Nature 292*, 81−82.
Rodgers, K. R., Su, C., Subramaniam, S., & Spiro, T. G. (1992) *J. Am. Chem. Soc. 114*, 3697−3709.
Rohlfs, R. J., Mathews, A. J., Carver, T. E., Olson, J. S., Springer, B. A., Egeberg, K. D., & Sligar, S. G. (1990) *J. Biol. Chem. 265*, 3168−3176.
Rousseau, D. L., & Friedman, J. M. (1988) in *Biological Application of Raman Spectroscopy* (Spiro, T. G., Ed.) Vol. III, pp 133−215, Wiley and Sons, New York.
Rousseau, D., Song, S., Friedman, J. M., Boffi, A., & Chiancone, E. (1993) *J. Biol. Chem. 268*, 5719−5723.
Scott, T. W., & Friedman, J. M. (1984) *J. Am. Chem. Soc. 106*, 5677−5687.
Sherman, D. R., Kloek, A. P., Krishnan, B. R., Guinn, B., & Goldberg, D. E. (1992) *Proc. Natl. Acad. Sci. U.S.A. 89*, 11696−11700.
Shiro, Y., Iizuka, T., Marubayashi, K., Ogura, T., Kitagawa, T., Balasubramanian, S., & Boxer, S. G. (1994) *Biochemistry 33*, 14986−14992.
Smerdon, S. J., Krzywda, S., & Wilkinson, A. J. (1993) *Biochemistry 32*, 5132−5138.
Spiro, T. G. (1988) in *Biological Application of Raman Spectroscopy* (Spiro, T. G., Ed.) Vol. III, pp 1−37, Wiley and Sons, New York.
Spiro, T. G., Smulevich, G., & Su, C. (1990) *Biochemistry 29*, 4497−4508.
Springer, B. A., Sligar, S. G., Olson, J. S., & Phillips, G. N., Jr., (1994) *Chem. Rev. 94*, 699−714.
Šrajer, V., Reinisch, L., & Champion, P. M. (1988) *J. Am. Chem. Soc. 110*, 6656−6670.
Stavrov, S. S. (1993) *Biophys. J. 65*, 1942−1950.
Stavrov, S. S. (1996) *Biophys. J. 70*, 1214−1223.
Stavrov, S. S. (1997) *Biophys. J. 72* (in press).
Valentine, J. S., Sheridan, R. P., Allen, L. C., & Kahn, P. C. (1979) *Proc. Natl. Acad. Sci. U.S.A. 76*, 1009−1013.
Wells, A. V., Sage, J. T., Morikis, D., Champion, P. M., Chiu, M. L., & Sligar, S. G. (1991) *J. Am. Chem. Soc. 113*, 9655−9660.
Wittenberg, B. A., Okazaki, T., & Wittenberg, J. B. (1965) *Biochim. Biophys. Acta 111*, 485−495.
Yang, J., Kloek, A. P., Goldberg, D. E., & Mathews, F. S. (1995) *Proc. Natl. Acad. Sci. U.S.A. 92*, 4224−4228.

BI971156N